Astron. Astrophys. 325, 305–317 (1997)

ASTRONOMY
AND
ASTROPHYSICS

# Quasi-separatrix layers in solar flares

## II. Observed magnetic configurations

**P. Démoulin**[1], **L.G. Bagalá**[2], **C.H. Mandrini**[2], **J.C. Hénoux**[1], **and M.G. Rovira**[2]

[1] Observatoire de Paris, DASOP, URA2080 (CNRS), F-92195 Meudon Cedex, France
[2] Instituto de Astronomía y Física del Espacio, IAFE, CC.67, Suc.28, 1428 Buenos Aires, Argentina*

Received 17 September 1996 / Accepted 2 December 1996

**Abstract.** We show that the location of H$\alpha$ or OV flare brightenings is related to the properties of the field-line linkage of the underlying magnetic region. The coronal magnetic field is extrapolated from the observed photospheric field assuming a linear force-free field configuration in order to determine the regions of rapid change in field-line linkage, called "quasi-separatrix layers" or QSLs. They are open layers that behave physically like separatrices: breakdown of ideal magnetohydrodynamics and release of free magnetic-energy may occur at these locations when their thickness is small enough. A feature common to all the flaring regions studied is found to be the presence of QSLs where H$\alpha$ flare kernels are observed. The brightenings are along restricted regions of very thin QSLs; an upper bound of their thickness is 1 Mm but it is several order of magnitude smaller in most of the cases. These places coincide in general with zones where the longitudinal field component is greater than 100 G. These results allow us to constrain present models of solar flares and localise where a break-down of ideal MHD can occur. The studied flares are found to be fed in general by only one electric current loop, but they imply the interaction of two magnetic bipoles. The extrapolated coronal field lines involved in the process have their photospheric footpoints located at both sides of QSLs, as expected in recent 3D magnetic reconnection models.

**Key words:** Magnetohydrodynamics (MHD) – Sun: flares – Sun: magnetic fields

### 1. Introduction

A still open debate about the way magnetic reconnection should work in 3D has arisen in the last years: do some 2D and $2\frac{1}{2}$D properties extend to 3D configurations or are the 2D and $2\frac{1}{2}$D cases so singular that a new theory, including other properties not revealed in previous analyses, needs to be constructed? The 2D and $2\frac{1}{2}$D approaches to reconnection are singular, in the sense that 2D and $2\frac{1}{2}$D reconnection can be defined in several ways that cannot be directly generalized to 3D. Basically 2D and $2\frac{1}{2}$D reconnection theory is intimately linked to separatrices and to their intersection (the separator). Hesse & Schindler (1988) have shown that separatrices are structurally unstable features because they disappear when slightly perturbing a $2\frac{1}{2}$D configuration to a 3D one. In their view, 3D reconnection can occur at any location provided that there is a break down of idealness. Another point of view has been given by Priest & Forbes (1989) who proposed that the imposed boundary flows select the particular line where reconnection takes place. On the other hand Bagalá et al., 1995; Démoulin et al., 1993, 1994; Mandrini et al., 1991, 1993, 1995; van Driel-Gesztelyi et al., 1994 show that the location of the energy release site is associated with the topology of the coronal magnetic field. In these works the photospheric field is extrapolated to the corona using a series of subphotospheric magnetic sources and the method, called Source Method (SM), used to determine the location of separatrices, is based on the connectivity between the sources.

However, the SM intrinsically needs the description of the magnetic field by subphotospheric sources. Priest & Démoulin (1995) have explored a way of generalizing the concept of separatrices to magnetic configurations without field-line linkage discontinuities. They propose that magnetic reconnection can also occur in 3D in the absence of null points at "quasi-separatrix layers" (QSLs), which are flat volumes where there is a rapid change in field-line linkage. They give an example of a sheared X-field where nearly any smooth and weak flow imposed on the boundary produces strong flows at the QSLs. Their results have been extended to typical theoretical flaring configurations built by four magnetic sources (Démoulin et al., 1996b, hereafter Paper I) and an algorithm, called QSLM (for quasi-separatrix layers method), has been developed in order to determine the locations of QSLs. The QSLM finds elongated regions that are in general located along small portions of the separatrices defined by the SM, and, in the limit of very concentrated photospheric fields, both methods give the same result (exept for the regions

*Send offprint requests to*: P. Démoulin
* Member of the Carrera del Investigador Científico, CONICET

where field lines are tangent to the photosphere). In bipolar magnetic configurations, the trace of QSL at chromospheric level are formed by two elongated regions located at both sides of the longitudinal inversion line, while in quadrupolar configurations four appear. The thickness of QSLs has been shown to be determined by the character (bipolar or quadrupolar) of the magnetic region, the intensity of the coronal currents and by the size of the photospheric field concentrations.

The next step, presented in this paper, is to apply the QSLM to different observed flaring configurations and to compare its results to observed features like flare ribbons or flare kernels. The QSLM and the extrapolation technique are briefly described in Sect. 2. We study a variety of configurations, ranging from quadrupolar to bipolar and from nearly potential to sheared ones, in order to show that QSLs are indeed a feature common to all flaring regions. This is illustrated here by applying the QSLM to five regions selected from the set previously studied with the SM (Sect. 3). We then confront present flare models to our results (Sect. 4). We conclude that energy is released in flares by magnetic reconnection as described in the recent 3D theoretical developments (Sect. 5).

## 2. Description of the method used

### *2.1. Quasi-separatrix layers method*

Following Priest & Démoulin (1995) and Paper I, the classical separatrices can be generalized to QSLs. These are regions where a drastic change in field-line linkage occurs, i.e. where field lines initially close separate widely over a short distance. Let us integrate over a distance $s$ in both directions the field line passing at a point P$(x, y, z)$ of the corona. The end points of coordinates $(x', y', z')$ and $(x'', y'', z'')$ define a vector $\boldsymbol{D}(x, y, z) = \{X_1, X_2, X_3\} = \{x'' - x', y'' - y', z'' - z'\}$. A drastic change in field-line linkage means that for a slight shift of the point P$(x, y, z)$, $\boldsymbol{D}(x, y, z)$ varies greatly. The function $\tilde{N}$, defined by

$$\tilde{N}(x, y, z, s) = \sqrt{\sum_{i=1,3} \left[ \left( \frac{\partial X_i}{\partial x} \right)^2 + \left( \frac{\partial X_i}{\partial y} \right)^2 + \left( \frac{\partial X_i}{\partial z} \right)^2 \right]}, \quad (1)$$

allows us to locate the region with a drastic change in connectivity for a given value of $s$. In the case of solar flares, as discussed in Paper I, the distance $s$ to be used is the distance to the photosphere (located at $z = 0$ here). Besides, since we are working in the approximation of an abrupt transition from a low to a high $\beta$ plasma ($\beta$, ratio of the plasma to the magnetic pressure) and of high magnetic Reynolds number, line-tying is imposed at the photospheric level and the location in that plane of field-line footpoints is a function of $x$ and $y$ only. Therefore, the function $\tilde{N}$ simplifies to:

$$N(x, y) = \sqrt{\sum_{i=1,2} \left[ \left( \frac{\partial X_i}{\partial x} \right)^2 + \left( \frac{\partial X_i}{\partial y} \right)^2 \right]}. \quad (2)$$

$N(x, y)$ is defined only on the boundary and is the norm of the displacement gradient tensor defined when mapping, by field lines, points from one section to another of the photosphere. The locations where $N(x, y)$ takes its highest values define the field lines involved in the QSLs. By following these lines we can locate the coronal portion of the QSLs. We refer the reader to Paper I for a discussion of the properties of $N(x, y)$ and of the basic characteristics of QSLs.

The SM, used previously to determine the locations of separatrices, requires the use of the magnetic field generated by sub-photospheric sources (because it is the change of the magnetic link betwen the sources which determine the separatrices). This is not compelling with the QSLM that can be used with any kind of magnetic field description. There is no longer a need either to precise how the observed field concentrations are grouped together or to integrate magnetic field lines below the photosphere. The QSLM permits to detect a separatrice as special case of QSL where its thickness is only limited by the spatial precision of the field-line integration. In particuliar, the QSLM permits to find separatrices associated to magnetic field-lines tangent to the boundary while the SM cannot (see paper I).

### *2.2. Extrapolation of the photospheric field*

The photospheric longitudinal field ($B_l$) has been extrapolated to the corona, under the linear force-free field assumption (constant $\alpha$), using the discrete fast Fourier transform method as proposed by Alissandrakis (1981). This method takes into account the position of the active regions (ARs) on the solar disk (the transformation of coordinates from the observed frame to the local one is explained in Appendix A). The best value of $\alpha$ is determined by fiting the observed shear in the H$\alpha$ fibrils and transverse field in the flare region.

In previous studies (see references in the Introduction) sub-photospheric magnetic poles or dipoles have been used to extrapolate the observed photospheric magnetic field to the corona. The SM method uses explicitly only sub-photospheric sources while the QSLM can use any representation of magnetic fields. We compare in this paper results obtain with Fourier transform with those obtain with sub-photospheric sources (both with a linear force-free field assumption). A model using a small number of sources is appropriate for computing QSLs when the magnetogram has well defined polarities, like in the case of AR 2372 (compare Fig. 1b to Fig. 1e). The method is still satisfactory when the magnetogram presents extended polarity regions as in AR 2776, though the best agreement between QSLs and H$\alpha$ brightenings has been found using the Fourier transform extrapolation (compare Fig. 3a,b and f).

The use of sources to extrapolate photospheric magnetograms has two main advantages. First, it allows us to take into account a large flux imbalance in the magnetic data. Second, the noise in the data is strongly decreased by a least-square fitting of the model to the observed magnetogram. The main disadvantages of using sources are that the model requires time to introduce interactively a great number of sources in the case

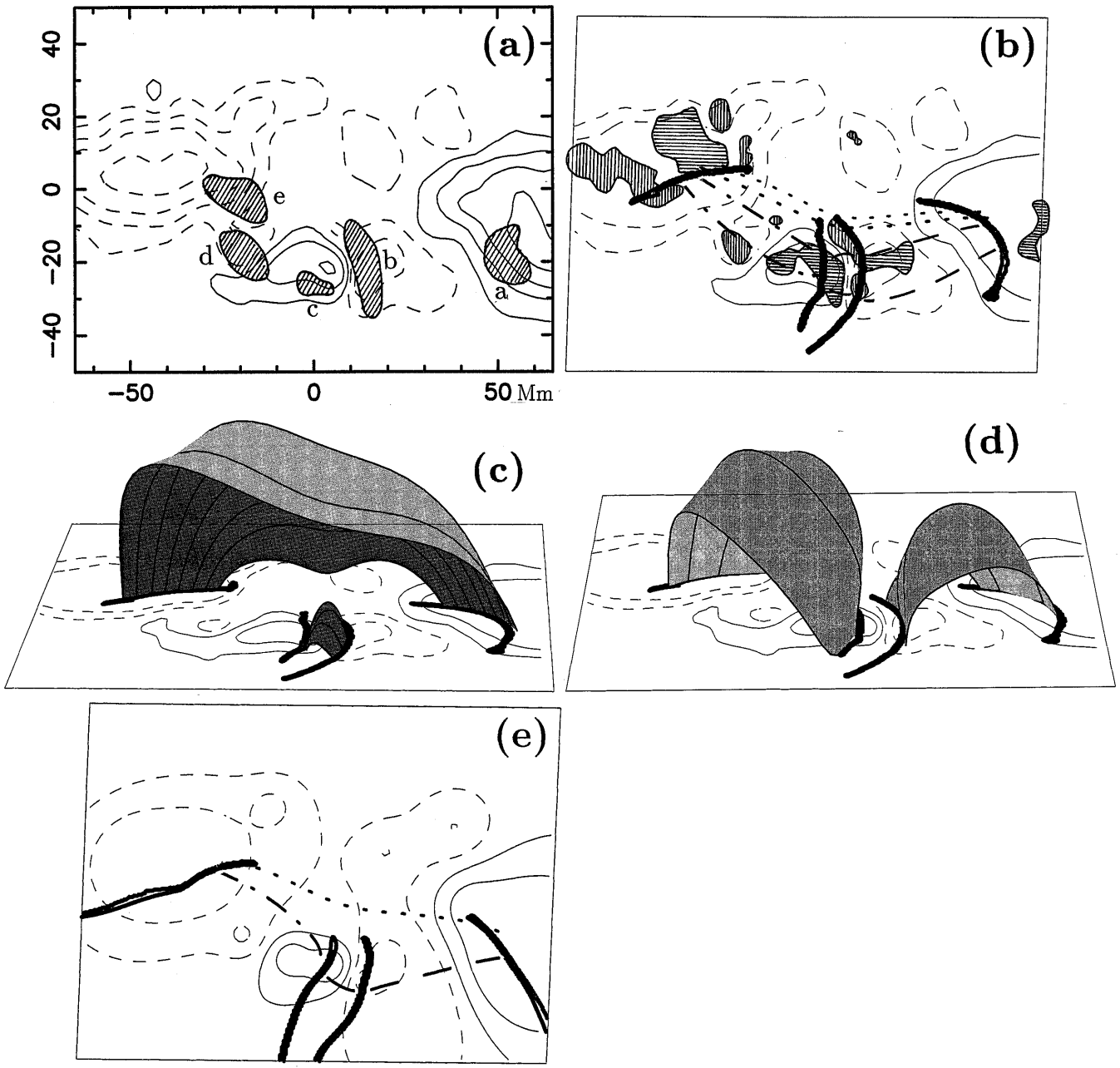


**Fig. 1a–e.** Flaring AR 2372 on April 6, 1980: example of quadrupolar region formed by the emergence of a small bipole with a polarity reversed from the main one. **a** Observational data: H$\alpha$ kernels (hatched regions labelled a, b, c, d and e) and longitudinal field $B_l$ (isocontours of $\pm 100, 400, 800, 1600$ G, with positive and negative values drawn with solid and dashed lines respectively). **b** Intersection of the QSLs with the photosphere (thick isocontour lines of $N = 10$) for a potential extrapolation of $B_l$ (isocontours $\pm 100, 400$ G of $B_l$ are added for reference). The coronal links between H$\alpha$ brightenings are given by four kinds of field lines. The regions where the vertical current density is greater than 10 mA m$^{-2}$ are marked with horizontal (resp. vertical) hatching for positive (resp. negative) values. **(c,d)** Perspective view of Fig. 1b showing the coronal linkage at the borders of QSLs with field lines drawn as surfaces (for aesthetics the vertical scale has been multiplied by a factor 3 compared to the horizontal one). The isocontours $\pm 100, 400$ G of $B_z$ (vertical field component) are added. **e** Same as in b but for a model with 12 magnetic sources. The sides of the Figs. 1a (resp. 1b-e) are parallel to the local $x, y$ axes (resp. observer $\xi', \eta'$ axes) as defined in Appendix A.

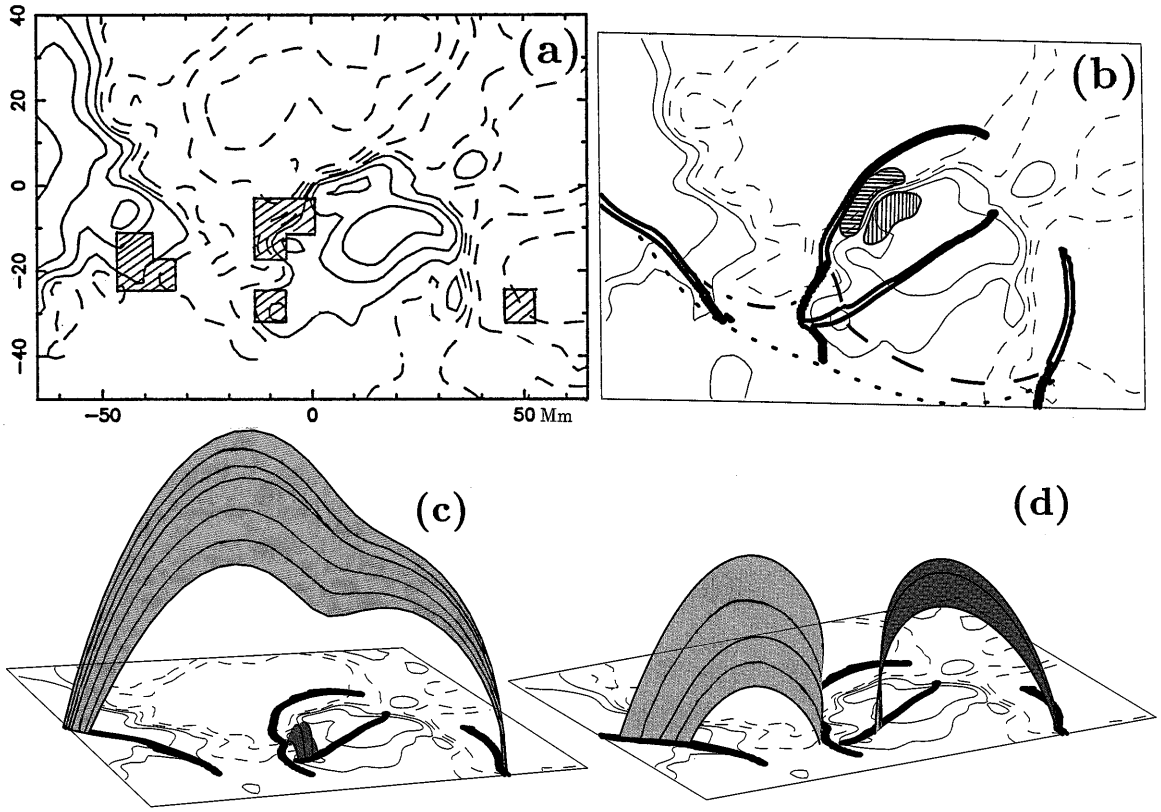


**Fig. 2a–d.** Flaring AR 2779 on November 12, 1980: example of quadrupolar region formed by two extended bipoles. The drawing convention is the same as in Fig. 1. **a** Observational data: OV kernels and longitudinal field $B_l$. **b** Intersection of the QSLs with the photosphere for a linear force-free extrapolation of $B_l$ ($\alpha = -0.019$ Mm$^{-1}$) with field lines and current-density regions. **c,d** Perspective views of **b**, with field lines drawn as surfaces.

of complex ARs, and that the description of the magnetic field by a series of sources is limited to linear force-free fields.

The Fourier transform is a more classical technique which takes into account the full magnetogram. The noise in the data can be easily decreased by filtering the higher harmonics, however this leads to a broadening of the magnetic polarities and this goes against a good computation of QSLs, since the distribution of the photospheric field in several concentrations is the origin of QSLs (in particular in bipolar regions). Without this filtering, strange connectivity patterns may be found. This is illustrated in Figs. 4, field lines link the external borders of QSLs that lie in zones where $B_l \geq 100G$ in Fig. 4b, while in Fig. 4c field lines issued from the inner borders of QSLs reach the photosphere at places where the noise in the data is close to 50G. We choose to use the data without filtering and restrict our attention to magnetic field greater than 100 G. The main limitations of the Fourier-transform extrapolation are: imposed flux balance, periodicity of the solution in the horizontal $(x, y)$ directions, proportionality between the current density and the magnetic field (through a constant called $\alpha$) and the restriction of application to ARs with low magnetic shear.

The errors associated with the use of a discrete fast Fourier transform can be inferred by simulating a magnetogram using magnetic sources and, then, comparing the results of the extrapolation of the simulated photospheric field to the model field. We have found that the locations of QSLs differ by less than the magnetogram resolution. The main limitation of the extrapolation is therefore the linear force-free field hypothesis. The limitations of the extrapolation scheme and the implications of the numerical precision on the location of QSLs and their thickness are further described in Appendix B.

## 3. In what type of magnetic configurations do flares occur?

### *3.1. QSLs in flaring configurations*

Compared to previous analyses of the flaring regions, we apply here two new methods both for the extrapolation of the observed field and for the topology computation. Because these methods use directly the magnetograms, a more accurate position of QSLs (as compared to the separatrices computed before) can be expected to lead to some progress in the understanding of the flaring mechanism. The performances of the new methods are illustrated below by application to four flaring regions (and a fifth one in Appendix A).

– AR 2372, located at N12 E08 on April 6, 1980, is a typical quadrupolar region where a small and less intense bipole emerged in between a larger one with a reversed polarity (Man-

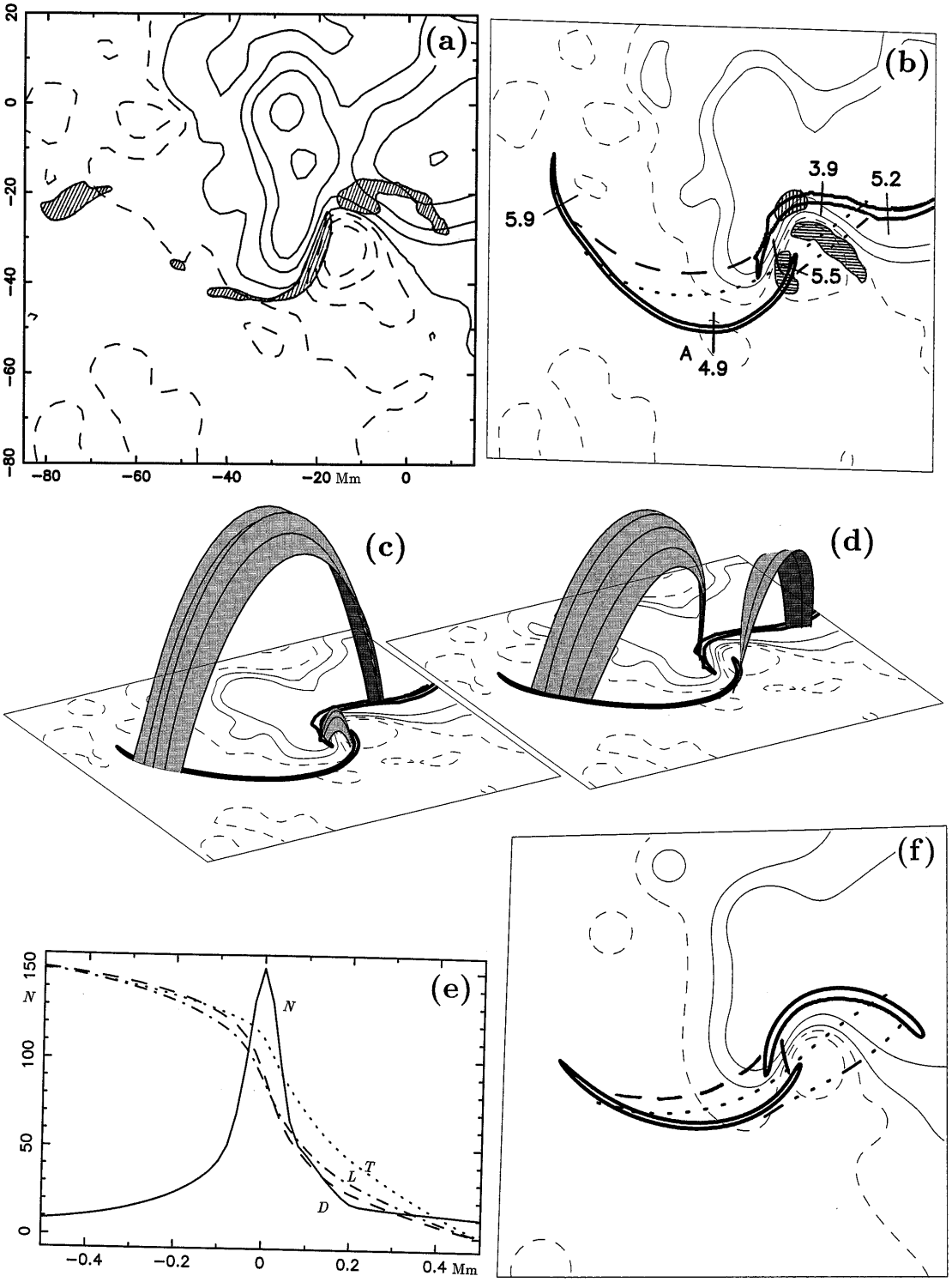


**Fig. 3a–f.** Flaring AR 2776 on November 5, 1980: example of a bipolar region with an S-shaped inversion line. The drawing convention is the same as in Fig. 1. **a** Observational data: H$\alpha$ kernels and longitudinal field $B_l$ **b** Intersection of the QSLs with the photosphere ($N$ = 10) for a linear force-free field extrapolation of the longitudinal field ($\alpha = -0.025$ Mm$^{-1}$). The numbers correspond to the decimal logarithm of the thickness (in meters) of the QSL at that location. Field lines and current-density regions are added. **c,d** Perspective view of Fig. 3b with the typical field lines (drawn as surfaces) on both side of QSLs. **e** Plot along a segment orthogonal to the QSL at point A (see Fig. 3b) of the function N (continuous curve), the distance $D$ between the field line footpoints (dashed curve), the field line length $L$ (dashed dotted curve) and the delay function $T = \int ds/B$ (dotted curve). The curves of $D, L, T$ have been normalized to their minimum and maximum values in the range considered. **f** Same as Fig. 3b but for a model using 18 magnetic sources.

drini et al., 1991). Five H$\alpha$ flare kernels are present, labelled a–e in Fig. 1a. Kernels a and e are in regions where no strong deviation from a potential field is observed, while there is a strong localized shear in the region of kernels b and c. Kernel d is located where a new small bipole, that started emerging on this day, was observed on April 7 and 8. This emergence could have been the origin of flaring in this zone as discussed by Mandrini et al. (1993), but it is at the spatial-resolution limit of the magnetogram so we do not comment further on this kernel. Within the limitations of a linear force-free approach, the topology of AR 2372 is not very sensitive to $\alpha$ so we present the extrapolation with a potential approximation. It can be seen that the main four H$\alpha$ kernels (a, b, c and e) lie on QSLs or at a distance from them smaller than the accuracy in the relative positioning between magnetic data and H$\alpha$ filtergrams, considered of about 2 magnetogram pixels or $\approx$ 4 Mm. Besides, they can be linked by field lines (Figs. 1b–d).

– AR 2779, located at S13 W06 on November 12, 1980, is another example of quadrupolar region (see Bagalá et al., 1995 for a detailed study). The analyzed flare presents four kernels observed in OV (Fig. 2a). In this case the two bipoles in the configuration have approximately the same magnetic intensity. Strong magnetic shear is present along the longitudinal inversion line in the intermediate bipole and also at the location of the two most distant flare kernels. This departure from potential is taken into account, on average, in the coronal extrapolation of the observed photospheric field. Again the four kernels are located on QSLs and can be linked by magnetic field lines (Fig. 2b–d).

– AR 2776, located at N11 E07 on November 5, 1980, is a typical bipolar region where the longitudinal inversion line has an "S" shape (Fig. 3a). Strong magnetic shear is observed along the inversion line where the small southern polarity is located, while the direction of chromospheric fibrils indicates a departure from potential in the preceding and following polarities (see Démoulin et al., 1994). In order to explain the location of the two elongated H$\alpha$ flare ribbons, this shear should be included in the extrapolation because the location of QSLs in bipolar configurations is more sensitive to magnetic shear than in quadrupolar ones. Notice, in particular, the case of the longer ribbon to the left which has only a QSL counterpart if the right shear is considered in the model (compare Figs. 3a to 3b). The connectivity between flare brightenings, shown in Figs. 3c and 3d, is similar to that of quadrupolar regions.

– AR 2511, located at N20 E00 on June 15, 1980, is a bipolar region where the inversion line is nearly straight and the observed magnetic field is nearly potential (at least in the strong field regions where B$>$ 200G, see Démoulin et al., 1993). All the computed field lines are nearly parallel and this region seems at first sight to have a very simple topology, a magnetic arcade-like one. However, the concentration of the photospheric magnetic field makes the 3D connectivity more complex: QSLs are even present in such simple bipolar region; they are located on the two left H$\alpha$ kernels while the "U" QSL on the right is shifted by appromimativelly of 8 Mm and slightly rotated from the right H$\alpha$ kernel (Fig. 4a,b). In the present computation we are able to link the H$\alpha$ ribbons by field lines only if the starting point is located on the external part of the QSLs, while field lines starting from the internal part end-up rapidly inside (Fig. 4c). This is our worst studied example, principally because the two interacting bipoles are nearly parallel so that the QSL positions are strongly influenced by the location of coronal currents. Moreover, the internal bipole (emerging flux) has a low magnetic flux so the magnetic-field measurements are difficult there. The present computation refers rather to the relaxed state where the field is nearly potential. The difference in position between the H$\alpha$ ribbons and QSLs is then interpreted as due to the evolution of the magnetic configuration from a twisted-flux tube emerging in the large scale bipole to a more arcade-like configuration with weaker electric currents.

### *3.2. Thickness of quasi-separatrix layers*

Inside the QSLs, shown as an isocontour of $N$ in Figs. 1 to 4, this function has much higher values in very thin and elongated regions. As it is numerically very expensive to resolve the variations of $N$ for the whole AR, we study the behaviour of this function cutting the QSL with a segment orthogonal to it at some localized points. The thickness, $\delta$, of a QSL is defined as the width of the function $N$ at half-height. In the absence of magnetic null points or of field lines touching tangentially the photosphere, a QSL has a finite thickness. How thin can it be in a flaring configuration? We have found in all the cases, QSLs thinner than the magnetogram resolution ($\approx$ 2 Mm). Does this numerical "super-resolution" have a meaning? The thickness of QSLs, like their locations, come from global properties of the magnetic configuration derived from field-line linkage. In Appendix B we show that the thickness magnitude of a QSL can be determined only if the magnetogram and the numerical grid for the extrapolation resolves the photospheric field concentrations.

Our analysis of the thickness at different places along the QSLs shows that, for the two quadrupolar regions (AR 2372 and AR 2779), the values of $\delta$ go down to the computer precision at the location of flare brightenings (with thickness lower than 1 m !). This means that in these ARs QSLs behave physically like separatrices. For bipolar ARs (AR 2776 and AR 2511) the values of $\delta$ turn out to be much higher (see Figs. 3b and 4b), in agreement with the results found for simple theoretical configurations in Paper I. The largest value of $\delta$ ($\approx 10^6$ m) corresponds to the left extreme of the left ribbon in AR 2776. Fig. 3e shows the typical behaviour of $N$ when the QSL thickness can be numerically resolved. In this figure we have also included, for completeness, three other functions that have a theoretical interest in understanding 3D magnetic reconnection (see Paper I for further comments). These are: the distance ($D$) between the photospheric footpoints of field lines, the field-line length ($L$) and the delay function or flux tube volume ($T = \int ds/B$, where the integration is performed along a magnetic field line). For the flaring configurations studied, like for the theoretical ones considered in Paper I, these three functions have similar shapes and sharp variations on the scale length of the QSL thickness; however, QSLs are better defined in terms of $N$ (see Paper I).

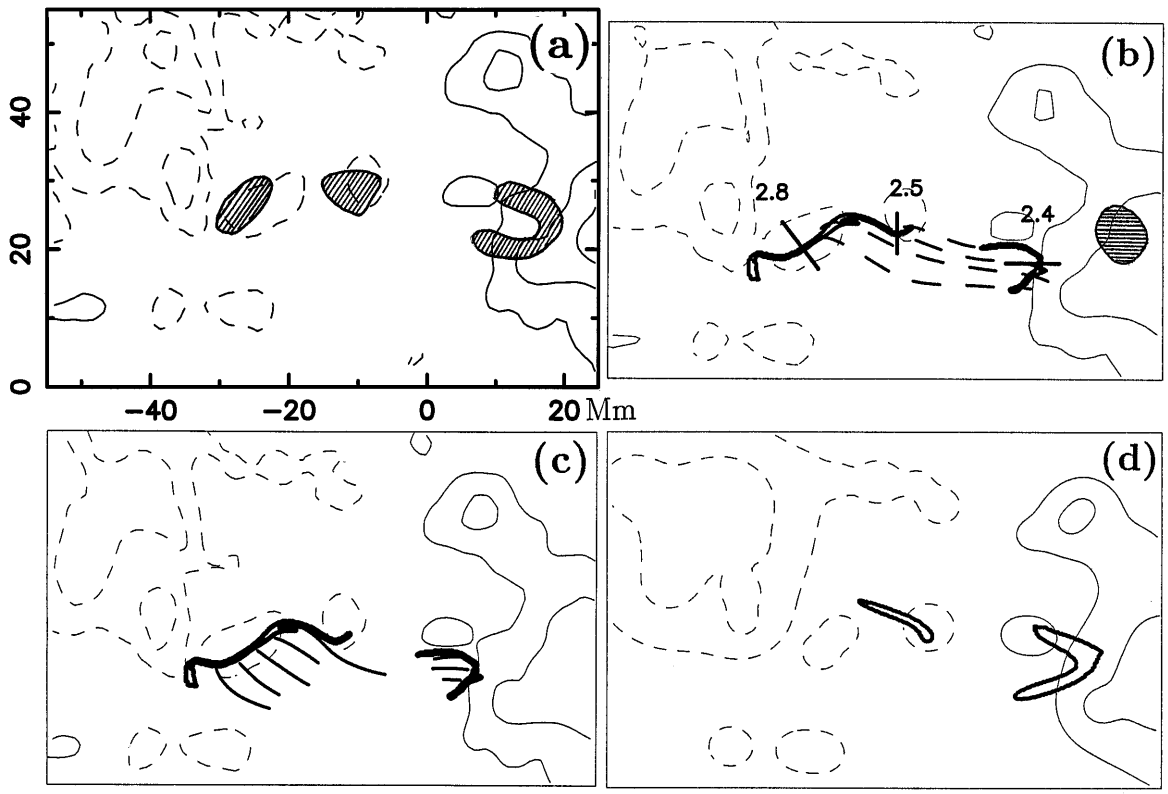


**Fig. 4a–d.** Flaring AR 2511 on June 15, 1980: example of a bipolar AR formed by the emergence of a small bipole having the same orientation as the main one. The drawing convention is the same as in Fig. 1. **a** Observational data: H$\alpha$ kernels and longitudinal field $B_l$. **b,c** Intersection of the QSLs with the photosphere ($N$ = 10) and some field lines for a linear force-free field extrapolation of $B_l$ ($\alpha = -0.006$ Mm$^{-1}$). In **b** the numbers have the same meaning as in Fig. 3b; the region where the current-density is greater than 5 mA m$^{-2}$ is marked. **d** Same as Fig. 4b but for a model using 28 magnetic sources.

### *3.3. Electric currents*

The vertical photospheric currents have beeen computed from the transverse magnetic field measurements (see references in Sect. 3.1). For almost all the studied ARs two photospheric current kernels of opposite sign, linked in the corona by field lines lying close to the computed separatrices, were found. This result remains with the Fourier transform extrapolation and the QSLs computation, as shown in Figs. 1b, 2b, 3b and 4b (in this last case only the current in the preceding polarity is detected above the noise level because the transverse field in the following polarity is too low). This indicates that the energy is presumably stored in these field-aligned currents and released during the flares. This result is remarkable since with both type of extrapolation are linear force-free so they do not take into account such concentration of the electric currents. Due to the Ampere's law the magnetic field created outside a current does not depend precisely on the current distribution so that the QSL deduced here are expected to be located close to the one deduced by a non-linear force-free field extrapolation.

However, we cannot deduce the local behaviour of field lines associated to the concentrated currents from linear force-free field extrapolation. The total twist of the field lines surrounding the current loop can be estimated by neglecting the curvature of the loop (because of a low aspect ratio) and by assuming a cylindrical symmetry. Then, following Amari et al. (1991, Sect. 6.3) the number of turns $n_t$ of the field lines at the periphery of the current loop can be estimated as:

$$n_t \approx \frac{\mu_0 I L}{4\pi F} ,$$

where $I$ is the total current, $F$ the magnetic flux and $L$ the length of the loop. For the regions studied we have estimated $I/F$ and $L$ for each magnetogram, what gives $n_t$ in the range [0.2, 0.5]. Of course these values have to be taken with caution because of the simple estimate made, but also because the calculation of the electric currents using transverse field measurements is problematic with the present magnetographs (see e.g. Gary and Démoulin, 1995, for a detailed description of the difficulties). Nevertheless, these low twist values are consistent with the absence of prominences in the studied flares (which are likely to be supported at the bottom of magnetic twisted flux tubes) and with the absence of ribbons with an "umbrella hand" shape which appear only when the twist is greater than one turn (Démoulin et al., 1996a).

## 4. Implications for flare models

The finding that flare kernels are located on QSLs and that they are linked by field lines extending along them, together with the presence of a system of electric currents, brings new light on the flare mechanism. This section intends to put the results found with the QSLM within the framework of our present knowledge of this mechanism.

### *4.1. Flaring loop models*

Flare loop models invoke a plasma micro-instability in a single magnetic loop when the electric current is too large (e.g. Alfvén & Carlqvist, 1967) or an ideal instability when the twist is too large (e.g. Mikić et al. 1990). Since we show that more than one simple loop is involved in the studied flares, our results do not support single-loop flare models. This is consistent with the low-twist of the current loop.

The present results seem to be in conflict with the "standard" image of solar flares which has emerged from observations aboard Yohkoh: one soft X-ray loop with a pair of footpoints and a top source in hard X-rays (Kosugi, 1994; Masuda, 1994; Masuda et al., 1995). However, two interacting loops are also often observed in soft X-rays in flares (Inda-Koide, 1994; Dennis et al., 1994, Hanaoka, 1995) and interacting multiple loops are an important fraction ($\approx$ 40%) of the transient brightenings observed in ARs (Shimizu et al., 1994). Besides multiple sources in hard X-rays are not a negligible fraction ($\approx$ 30%) of the observed flares (Sakao et al., 1994) and some remote hard X-ray sources linked to the flare loops are not seen in soft X-rays, but appear bright in microwaves (e.g. Yaji et al., 1994). Interaction between loops is also observed in the corona in Fe lines (Smartt et al., 1993).

There are, at least, three reasons that can explain why only a single loop is seen in soft X-rays. First, as single-loop events are found to be smaller in extension (usually less than 20 Mm) than multiple-loop events (Shimizu et al., 1994), the observation of single-loop events can be due to a lack of spatial resolution (Shimizu et al., 1994). Second, in bipolar regions the two reconnected loops are close together and can be easily taken as one loop (see Figs. 3b, 4b for example). Third, even in quadrupolar regions where the X-ray loops are well separated, a large difference in size between them implies a large difference both in energy input per unit of volume and in density enhancement (e.g. due to evaporation). This implies that the longer loop, much less bright, can be overlooked, in particular if the time exposure is chosen for not overexposing the short bright loop. Such situation occurs when a small magnetic bipole impacts into a much larger one (see e.g. Mandrini et al., 1996). In hard X-rays there are also several reasons for missing some sources: the evolution of the hard X-ray sources during the flare from the feet to the top of loops (e.g. Yaji et al., 1994), the field strength difference between the feet of the loops implying different mirroring conditions of particles (Sakao et al., 1994), the anisotropy in the injection of particles, and finally only two X-ray footpoint sources are expected in bipolar regions.

While the spatial resolution is better for H$\alpha$ observations, a direct analysis can also falsely support a single-loop flare model. Because H$\alpha$ kernels are located inside the feet of X-ray loops, it is natural to find the counterpart of the three points listed above. First, for some small flares, the H$\alpha$ observations may not have the resolution required to visualize the ribbons (for example kernel d in Fig. 1). Second, in bipolar regions, two ribbons are expected while four kinds of field-line linkages exist like in quadrupolar regions (e.g. Fig. 3). Third, some less intense kernels may be overlooked. In this sense the computation of QSLs is a useful tool to find the relevant features related to a given flare (for example, the faintest UV kernel in November 12, 1980 flare was found when looking for it in the zone close to the computed separatrices, see Bagalá et al., 1995).

### *4.2. Magnetic reconnection: a common feature to flares*

In the set of events studied previously only one well-defined current loop associated to the flares was found. In AR 2372, a second current loop is present in the main bipole but its foot in the preceding spot is not located in the vicinity of the QSL (Fig. 1b). Moreover, this current evolves drastically from April 6-8 while homologous flares are observed (Mandrini et al., 1993). This main-bipole current seems then not to take part in the flaring process. Therefore, none of the studied flares appears to occur because two current loops attract as proposed in the current-loop coalescence models (e.g. Sakai & De Jager 1996, and references therein).

An emerging flux model for flares was proposed by Heyvaerts et al. (1977), being further investigated by Forbes & Priest (1984). The magnetic configurations of April 6-8 and June 13-15, 1980 are cases where this model can be applied. The eruption of a twisted flux-tube (e.g. Priest 1982, p. 367) is another candidate to induce flaring. The absence of a prominence eruption is not a problem for this model because the low $\beta$ plasma in the prominence has a negligible influence on the magnetic field. The main problem of the twisted flux-tube model, in the case of the confined flares studied, is rather the absence of a twisted configuration in the extrapolated coronal field. Of course this can be due to the intrinsic limitations of the extrapolation method (which cannot include the concentrate currents observed at the photosphere), but the fact that we find the flare kernels on QSLs shows that the extrapolated configuration is realistic. Moreover, the electric currents, measured directly from the transverse field, are not intense enough to form a twisted flux-tube and the flare ribbons have not the characteristic shape ("umbrella hand" shape) present in twisted configurations (Démoulin et al., 1996a).

For the studied flares, the locations of flare kernels in relation to QSLs point out clearly a reconnection mechanism. Due to the intrinsic difficulties of the problem, magnetic reconnection has been studied mainly in 2D and $2\frac{1}{2}$D magnetic configurations (see Malherbe 1987 and Priest 1992 for reviews). In these models, energy release occurs on separatrices and, in particular, on their intersection; so the H$\alpha$ kernels should be located where separatrices cut the chromosphere. Four brightenings are

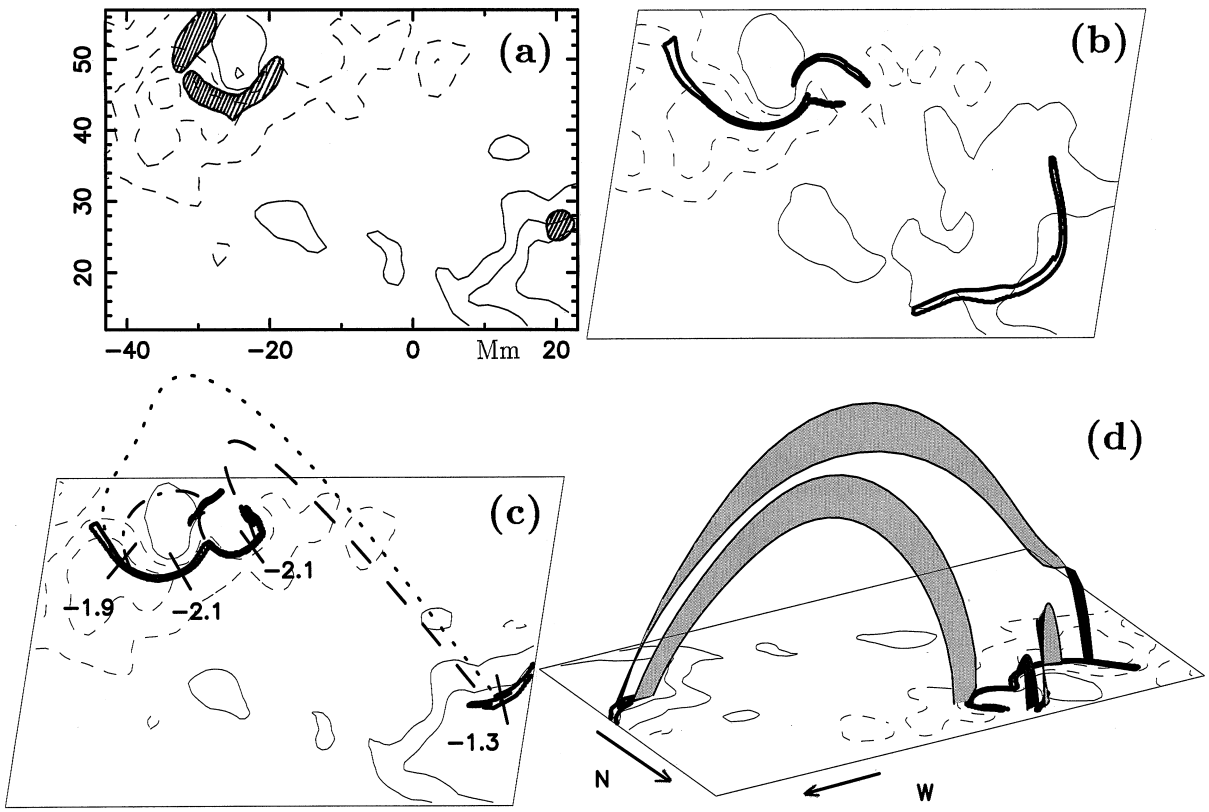


**Fig. 5a–d.** Flaring AR 2511 on June 13, 1980: example of a parasitic polarity embedded in the opposite polarity spot of the main bipole. The drawing convention is the same as in Fig. 1. **a** Observational data: H$\alpha$ kernels and longitudinal field $B_l$. **b** Intersection of the QSLs with the photosphere for a potential field extrapolation of $B_l$. The isocontours $\pm 100, 400$ G of the vertical field $B_z$ are added. **c** Intersection of the QSLs with the photosphere when only the spatial coordinates are transformed (the photospheric field is supposed to be vertical). Some field lines linking the kernels have been drawn. The logarithm of the thickness (in meters) of the QSL at some locations are marked. **d** Perspective view of **c** including typical field lines (drawn as surfaces) on both sides of QSLs. The photospheric plane has been rotated in order to show the shorter field lines.

expected in quadrupolar regions and only two in bipolar ones involving a twisted magnetic structure. Therefore, with a symmetry of translation, the configuration associated with four and two-ribbon flares is quite different: the first kind of flares involve the interaction of two bipoles and the second one supposes the formation of a twisted flux-tube. The possibilities of field-line connections are much larger in 3D. In Paper I we have shown theoretically that we can pass continuously from a case with four ribbons to a case with two. The observations confirm this view: flares are present in configurations where two bipoles are antiparallel (Fig. 1), or when they are less antiparallel (Figs. 2, 3, 5), or even nearly parallel (Fig. 4). In 3D magnetic configurations, two-ribbon flares do not need the formation of a twisted flux-tube and may happen even in bipolar regions having low magnetic shear, so apparently in a simple magnetic arcade. All the studied flares strongly support a model based on magnetic reconnection taking place in different configurations. Theoretical research in 3D magnetic reconnection has started few years ago, and at this point solar observations seem to support this growing-up theory !

### *4.3. Formation and release of the electric currents*

How are the current loops formed which are powering the flares? Based on the observations several ways have been proposed: by spot motions (e.g. Gesztelyi et al., 1986; Hanaoka, 1994), by photospheric twisting motions (e.g. Martres et al., 1970; Hénoux and Somov, 1996) or by emergence of twisted flux-tubes (Leka et al., 1996). In these cases a loop current is formed at some location in the AR and a flare occurs when the loop current reaches the QSLs. Another possibility, developed in Paper I, is that concentrated currents are naturally formed by any photospheric motion at QSLs. This is so because two neighboring field lines are subjected to different photospheric motions since their opposite footpoints are separated by a great distance and, therefore, electric currents with strong densities are created at QSLs. This gives a natural explanation to the results of Sect. 3.3; though only one current loop is detected above the noise level because the currents formed are stronger in the inner bipole where the photospheric velocities are larger. In fact, with the present data we cannot decide if the currents are transported to or formed in the QSLs; we need both a better time cover-

age with magnetograms and more accurate linear polarization measurements to follow the time evolution of the currents.

When QSLs are thin enough, magnetic energy release is possible at their location either because a current-density threshold is reached (Paper I) or because the field-line velocity becomes much larger than the plasma velocity (Priest & Démoulin 1995). This view is supported by the recent analysis of the temporal evolution of QSLs associated with an X-ray bright point: Mandrini et al. (1996) show that the QSL on the emerging bipole is very thin (typically less than 100 m) during the lifetime of the XBP, but becomes much thicker ($\geq 10^4$ m) after the XBP has faded. In some of the flaring regions studied here (AR 2372, AR 2779, AR 2511), the QSLs are thin enough to allow reconnection; but in some regions (e.g. AR 2776) the QSL thickness can be as large as 1 Mm ! We can interpret these results as follows: in flares, storage of magnetic energy is a necessary first step, contrasting with XBPs where the energy is released as soon as it is available. For such storage, a QSL thickness of the order of 1 Mm is enough to create concentrated currents (as observed). Then at some point the quasi-static evolution of the configuration cannot go on, because QSLs are becoming too thin, and a flare occurs. The influence of growing electric currents on QSLs remains to be investigated with a nonlinear force-free field extrapolation, but there are some analytical results that show that the QSL thickness decreases exponentially with increasing twist (Démoulin et al., 1996a).

## 5. Conclusion

When trying to understand very complex physical phenomena like solar flares, a strong interaction between observations and theory is certainly required. In particular, observations allow us to choose between all the possible models, which always oversimplify reality, and guide us in selecting the most relevant approximations. On the other hand, models help us in extracting the most relevant features from the mass of observations. Some years ago, we began to investigate the flare problem in this spirit. Magnetic reconnection seemed to be the most likely candidate for energy release during flares but the debate was, and still is, largely opened since 3D MHD modelsare needed. Due to the intrinsic difficulties to build up a time-dependent 3D model of the field with the observed data as boundary conditions, we restricted ourselves to the study of 3D magnetic field equilibria and we focussed our work on the spatial distribution of flare by-products.

The 2D and $2\frac{1}{2}$D studies of magnetic reconnection show the importance of separatrices, energy is released there giving as results plasma jets with high velocities and accelerated particles. At the time we began flare studies, following the work of Baum & Brathenal (1980) and Gorbachev & Somov (1988), the location of separatrices in 3D magnetic-field configurations was only known when the field was modeled using a set of sources. We further improved the method (called SM, for Source Method) by developing a numerical algorithm to find the separatrices, by fitting by least-squares the parameters of the sources to the observed data, by comparing charge and dipole representations and by taking into account the observed magnetic shear. This allowed us to show that, in very different configurations, both H$\alpha$ and UV flare kernels are linked to the topology of the active-region magnetic field (see references in the Introduction).

Since the SM is based on the magnetic linkage between subphotospheric sources, some readers may have some doubt on the results because flares are purely coronal events. We have then attempted to overcome this limitation (see Paper I) in several ways. In particular, we have found that flares are not necessarily associated to the presence of magnetic null points, nor to field lines tangentially touching the photosphere (or chromosphere). That is to say, that flares are not always related to the coronal separatrices in a classical sense. In Paper I we extended the notion of separatrices to the notion of quasi-separatrix layers (QSLs), which are regions where the field-line linkage is drastically changed. In theoretical configurations, we have shown that QSLs extend only along parts of the separatrices computed with the SM and we have described them in typical quadrupolar and bipolar regions.

In the present paper, we computed QSLs in flaring active regions, extrapolating the original observed photospheric field by a linear force-free field. We have found that the feature common to the various flaring regions studied is the presence of QSLs. The H$\alpha$ or UV kernels are found lying close to them in zones where the magnetic field is in general greater than 100 G. This confirms and precises previous results obtained with the SM, in the sense that flare kernels are not observed all along separatrices computed with the SM but only on the portion obtained when computing QSLs. Our finding precise the locations where ideal MHD can break down in the theory of Hesse & Schindler (1988). We have further shown that two-ribbon flares have basically the same field-line connectivity as flares with three or four ribbons. The studied flares are found to be fed by only one electric current loop but they imply interactions between several magnetic structures, and none of the studied flares correspond to a single flaring flux-tube. All the studied flares have a parasitic bipole located in between a main bipole. The main difference between these regions is the relative orientation of the two bipoles. These results confirm that flares are coronal events where the release of free magnetic-energy is due to the presence of regions where the magnetic field-line linkage changes drastically. They agree with the observational results of Yohkoh satellite (e.g. Tsuneta 1993, Hanaoka 1994, Masuda et al., 1994, Shimizu et al., 1994) obtained on a completely independent base and strongly support the hypothesis that 3-D magnetic reconnection is at work in solar flares, even if more theoretical investigations on the physics of 3-D magnetic reconnection are still needed.

*Acknowledgements.* We acknowledge financial support from the CONICET (Argentina) and CNRS (France) through their Argentina-France cooperative science program. We thank the referee Bert Van den Oord for his detailed comments which help to improve the readability of this paper. We thank Mona Hagyard, Jean Rayrole and Brigitte Schmieder for the magnetic field observations. P. D. thanks the staff at IAFE for his hospitality and C.H.M. thanks the staff at DASOP in turn.

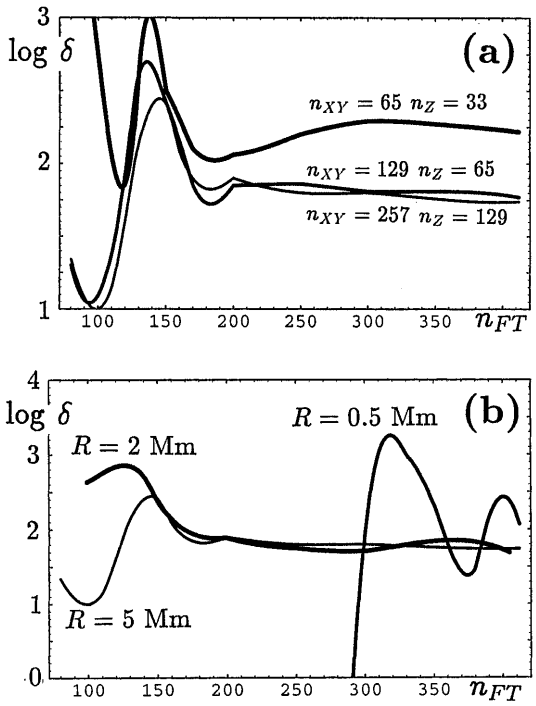


**Fig. 6a and b.** Evolution of the logarithm of the QSL thickness $\delta$ (in m) with the number of Fourier modes $n_{FT}$ for a theoretical configuration (see Appendix B). The three curves correspond to: **a** different resolution of the final non-uniform grid; **b** different radius $R$ of the photospheric flux concentration.

## Appendix A: off disk-centre transformations

The analysis of magnetograms taken away from the center of the solar disk requires the elimination of projection effects. This implies the transformation of both the measured vector magnetic field (Hagyard 1987) and the image plane spatial coordinates (Venkatakrishnan et al., 1988). The total transformation from the image coordinates $\xi, \eta, \zeta$ (where $\xi, \eta$ are parallel to the magnetogram axes and $\zeta$ is directed to the observer) to the heliographic coordinates $x, y, z$ ($x, y$ are the local horizontal coordinates, $x$ directed to the solar West, $y$ to the North and $z$ is the local vertical) has been given by Gary & Hagyard (1990). These authors show that the solar curvature can be neglected in the analysis of an AR if it is closer than $50^0$ from the centre of the disk. More precisely, for a region of 100 Mm width and located at $40^0$ from disk centre neglecting the curvature leads to a maximum position error of 2 Mm at its border, that is the typical size of a magnetogram pixel. Because the distance between H$\alpha$ kernels is in general less than 100 Mm, the solar curvature has a negligible effect on the relative positioning of the brightenings and the field topology.

The QSLs determined with and without the previous transformation lie very close for all the studied configurations except for AR 2511 on June 13, 1980. This AR was located at E26 N20 on that date and it is the farthest one from disk centre with which we have dealt. When the observed region is far from the centre of the disk, $B_l$ is a mixture of the vertical and horizontal field components, which can be separated only badly by the model because the photospheric field is not a force-free field. This fact is in particular important on June 13 region because the flare kernels (and QSLs also) associated to the following polarity are located in a weak field zone, while the ones associated to the preceding polarity lie on a more intense field. The resulting model shows a "laughing face" feature in $B_z$ located towards the left of the preceding spots (Fig. 5b). This is clearly an artifact because the magnetic data obtained on June 14 are not consistent with the existence of this positive flux zone (see Démoulin et al., 1993). Supposing that the photospheric field is nearly vertical, so that $B_z$ is proportional to $B_l$, and transforming only the spatial coordinates we obtain a more satisfactory result where QSLs are found close to flare kernels and extrapolated coronal field-lines link them like in all the other flares studied (Fig. 5c,d). Clearly, when the AR is far from the centre of the disk (say by more than $30^0$) we need a precise measurement and calibration of the transverse field together with a good resolution of the $180^0$ ambiguity so that the vertical field can be deduced (see Venkatakrishnan & Gary, 1989). When only the longitudinal component is available, it is better to suppose that the field is vertical than to use the longitudinal component as a boundary condition for the extrapolation.

## Appendix B: numerical precision on QSLs

Added to the errors in the magnetic calibration (when transforming the observed polarization in Fe lines to the magnetic field components) and to the spatial resolution of the magnetograph ($\approx$ 2 Mm), there are errors intrinsic to the extrapolation method. First, the photospheric magnetic field is measured in a region where it is not force-free, second the derived electric currents appear more concentrated than the ones resulting from a linear force-free field assumption, and third there are numerical errors due to the numerical method used. In the absence of precise chromospheric magnetograms, the first limitation can partially be overcome because the magnetic field becomes nearly force-free just above the photosphere (at a height of $\approx$ 400 km; see Metcalf et al., 1995) and the flux of the vertical component is approximately preserved. The second problem could be avoided using a nonlinear force-free extrapolation, but this is still a research domain (see e.g. Amari & Démoulin, 1992). We describe below the effects of the third limitation.

Magnetograms have usually a magnetic flux unbalance of a few $10\%s$. This unbalance can be taken into account in the Fourier transform extrapolation including the zero harmonic; but since this is a constant, implying an infinite energy in the field, we have decided to discard it. This change in the original data can be reduced by enlarging the size $L$ of the computed region to several times the size of the magnetogram. In practice, an enlargement by a factor 2 typically leads to a uniform modification of the data of less than 10 G. This enlargement is at the detriment of the maximum shear that can possibly be considered ($\alpha_{\max} = 2\pi/L$). For $\alpha$ larger than $\alpha_{\max}$, the large-scale harmonic solutions become periodic with height, implying again an infinite energy in the field. These solutions can be dis-

carded but the boundary conditions are then changed. We rather choose $\alpha < \alpha_{\max}$ and, therefore, restrict our analysis to magnetic regions which are not highly sheared.

When using a Green extrapolation method, the magnetic field is usually assumed to be zero outside the magnetogram. As mentioned in Sect. 2.2, with a discrete fast Fourier transform method the magnetic field is implicitly supposed to be periodic along two orthogonal horizontal directions $(x, y)$. In order to avoid aliasing errors (Alissandrakis 1981; see also Schmieder et al., 1990), due to the interaction between the studied region and its neighbour images, we take an integration area of side $L = L_x = L_y = 200$ Mm; that is to say twice the size of any typical magnetogram used here, the field being put to zero outside the observed region. As mentioned in the previous paragraph, this value of $L$ restricts the maximum shear that can be considered to $\alpha_{max} = 2\pi/L = 3.10^{-2}$ Mm$^{-1}$. For further properties of the method and comparison to others see Gary (1989).

Besides, when using the Fourier transform method, the magnetic field is computed on a uniform horizontal mesh at any height. In order to save computer memory, we keep the results in a non-uniform grid. The grid size is minimum at the centre of the integration area – let us call it $\Delta_{min}$ – and increases geometrically by a factor $c_{xy}$ towards the borders. The same kind of grid is used in the vertical direction $(z)$. In this direction the minimum spacing, taken as $\Delta_{min}$, starts at the photospheric level and the grid increases with height by a factor $c_z \approx c_{xy}$. The height of the integration volume is $L_z \approx L/2$. With this non-uniform mesh, we keep only a total number of points $n_{xy}^2 n_z$ much lower than $n_{FT}^3$.

We have seen in Sect. 3.2 that the thickness of the computed QSLs can be much smaller than the magnetogram resolution. We analyse now the influence of the discretization used on the properties of QSLs. With this aim, we build up a magnetogram formed by a bipolar background flux and by four flux concentrations of radius $R$ (we simply use a uniform field for both components). The $(x, y)$ coordinates in Mm for the positive concentrations are (40.,0.) and (60.,0.), while for the negative ones they are (0.,10.) and (0.,-10.). We take for this test $L = 2L_z = 400$ Mm, so that aliasing errors are negligible in the determination of QSLs. This theoretical configuration, still close to the observed ones, allows us to calculate the thicknesses of QSLs down to the precision of the computer (with a relative value lower than $10^{-12}$).

The evolution of the decimal logarithm of the QSL thickness ($\delta$) in meters as a function of $n_{FT}$ (Fig. 6a) shows that more than 200 Fourier modes (in one direction) are required to obtain meaningful results (i.e., we need to resolve the photospheric polarities: $L/n_{FT} \preceq 2$ Mm, being the radius of the flux concentrations $R = 5$ Mm). For the non-uniform grid with a number of points $n_{xy} = 65$ and $n_z = 33$ (leading to $c_{xy} = c_z \approx 1.1$ with $\Delta_{min} = 1$ Mm) we have only approximate results, but $n_{xy} = 129$ and $n_z = 65$ ($c_{xy} = c_z \approx 1.03$) are large enough and no significant differences are found with respect to a mesh twice finer ($n_{xy} = 257$ and $n_z = 129$, leading to $c_{xy} = c_z \approx 1.0065$; that is to say, a nearly uniform mesh). The influence of the flux-concentration radius is shown in Fig. 6b for the largest grid ($n_{xy} = 257$ and $n_z = 129$). The QSL thickness can still be obtained with a good precision for a flux concentration with a radius of 2 Mm ($\Delta_{min} = 0.5$ Mm for the figure) but not for a radius of 0.5 Mm ($\Delta_{min} = 0.2$ Mm), because $n_{FT}$ is not large enough (even for $n_{FT} = 412$, $R$ is two times smaller than $L/n_{FT}$).

The tests described above show that a QSL thickness much lower than the pixel size has a meaning. The numerical grid needs only to be fine enough to resolve the magnetic field spatial variations, so as to calculate the magnetic field lines correctly. In our computations we have found that, taking the maximum number of points allowed by the computer memory, we have a numerical grid fine enough compared to the magnetogram resolution. It is mainly the conversion from polarization to magnetic field, the magnetogram resolution and the physical equations used to model the coronal field, that limit the accuracy in the computation of the properties of QSLs. With these limits kept in mind, a more sophisticated extrapolation will give the coronal field on a numerical mesh, so it is important that the QSLs thickness can indeed be estimated for such numerical models.

## References


Alissandrakis C.E. 1981, A&A 100, 197

Alfvén H. & Carlqvist R. 1967, Solar Phys. 1, 220

Amari T., Démoulin P., Browning P., Hood A.W. & Priest E.R. 1991, A&A 241, 604

Amari T. & Démoulin P. 1992, in Proceedings of Workshop "Méthodes de détermination des champs magnétiques solaires et stellaires", Observatoire de Paris, p. 187

Bagalá L.G., Mandrini C.H., Démoulin P., Rovira M.G. & Hénoux J.C. 1995, Solar Phys. 161, 103

Baum P. & Bratenahl A. 1980, Solar Phys. 67, 245

Démoulin P., van Driel-Gesztelyi L., Schmieder B., Hénoux J.C., Csepura G. & Hagyard M.J. 1993, A&A 271, 292

Démoulin P., Mandrini C.H., Rovira M.G., Hénoux J.C. & Machado M.E. 1994, Solar Phys. 150, 221

Démoulin P., Priest E.R. and Lonie D.P. 1996a, JGR 101, A4, 7631

Démoulin P., Hénoux J.C., Priest E.R. & Mandrini C.H. 1996b, A&A 308, 643 (Paper I)

Dennis B.R., Holman G.D., Hudson H.S., Kosugi T., Strong K.T.& Zarro D.M. 1994, Proc. of Kofu Symposium, NRO Report No. 360, 217

Forbes T. & Priest E.R. 1984, Solar Phys. 94, 315

Gary G.A. 1989, ApJ 69, 323

Gary G.A. & Démoulin P. 1995, ApJ 445, 982

Gary G.A. & Hagyard M.J. 1990, Solar Phys. 126, 21

Gesztelyi, L., Karlicky, M., Farnik, F., Gerlei, O. & Valnicek, B. 1986, in "The Lower Atmosphere of Solar Flares", ed. D.F. Neidig, Sacramento Peak, p. 163

Gorbachev V.S. & Somov B.V. 1988, Solar Phys. 117, 77

Hagyard M.J. 1987, Solar Phys. 107, 239

Hanaoka Y. 1994, ApJ 420, L37

Hanaoka Y. 1995, Solar Phys. 165, 275

Hénoux J.C. and Somov B. 1996, A&A in press

Hesse M. & Schindler K. 1988, JGR 93, A6, 5559

Heyvaerts J., Priest E.R. & Rust D.M. 1977, ApJ 216, 123

Inda-Koide M. 1994, Proc. of Kofu Symposium, NRO Report No. 360, 161

Kosugi T. 1994, Proc. of Kofu Symposium, NRO Report No. 360, 11
Leka K.D., Canfield R.C., Mc Clymont A.N. & van Driel-Gesztelyi L. 1996, ApJ 162, 547
Malherbe J.M. 1987, Thèse de doctorat d'état, Université Paris VII
Mandrini C.H., Démoulin P., Hénoux J.C. & Machado M.E. 1991, A&A 250, 541
Mandrini C.H., Rovira M.G., Démoulin P., Hénoux J.C., Machado M.E. & Wilkinson L.K. 1993, A&A 272, 609
Mandrini C.H., Démoulin P., Rovira M.G., de la Beaujardiére J.F. and Hénoux J.C. 1995, A&A 303, 927
Mandrini C.H., Démoulin P., Van Driel-Gesztelyi L., Schmieder, B., Cauzzi G.& Hofmann A. 1996, Solar Phys. 168, 115
Martres M.J., Michard R., Soru-Iscovici L. & Tsap T.T. 1968, Solar Phys. 5, 187
Martres M.J., Soru-Escaut I. & Rayrole J. 1970, in Solar Magnetic Fields, IAU 43, ed. R. Howard, p. 435
Masuda S. 1994, Proc. of Kofu Symposium, NRO Report No. 360, 209
Masuda S., Kosugi T., Hara H., Sakao T., Shibata K. & Tsuneta S. 1995, PASJ, 47, 677
Metcalf T.R., Jiao L., McClymont A.N., Canfield R.C. & Uitenbroek H. 1995, ApJ 439, 474
Mikić Z., Schnack D.D. and van Hoven G. 1990, ApJ 361, 690
Priest E.R. 1982 Solar Magnetohydrodynamics, D. Reidel, Dordrecht, Boston, Lancaster
Priest E.R. 1992, IAU Coll. 133, "Eruptive Solar Flares", eds. Z. Svestka, B.V. Jackson & M.E. Machado, Springer-Verlag, Lec. Notes in Phys. 399, p. 15.
Priest E.R. & Démoulin P. 1995, JGR 100, A12, 23443
Priest E.R. & Forbes T. 1989, Solar Phys. 119, 211
Sakai J.I. & De Jager C. 1996, Space Sci. Rev. 77, 1
Sakao T., Kosugi T., Masuda S., Yaji K., Inda-Koide M. & Makishima K. 1994, Proc. of Kofu Symposium, NRO Report No. 360, 169
Schmieder B., Dere K.P., Raadu M.A., Démoulin P. & Alissandrakis C.E. 1990, Adv. in Space Res. 10, 9, 195
Shimizu T., Tsuneta S., Acton L.W., Lemen J.R., Ogawara Y. & Uchida Y. 1994, ApJ 422, 906
Smartt R.N., Zhang Z. & Smutko M.F. 1993, Solar Phys. 148, 139
Tsuneta S. 1993, PASP Conf. Ser. 46, 239
van Driel-Gesztelyi L., Hofmann A., Démoulin P., Schmieder B. & Csepura G. 1994, Solar Phys. 149, 309
Venkatakrishnan P. & Gary G.A. 1989, Solar Phys. 120, 235
Venkatakrishnan P., Hagyard M.J. & Hathaway D.H. 1988, Solar Phys. 115, 125
Yaji K., Kosugi T., Sakao T., Masuda S., Inda-Koide M. & Hanaoka Y. 1994, Proc. of Kofu Symposium, NRO Report No. 360, 143.

This article was processed by the author using Springer-Verlag LaTeX A&A style file *L-AA* version 3.